Physical Optics Computer Code Optimized for Synchrotron Radiation

Oleg Chubar, Pascal Elleaume, Serguei Kuznetsov, Anatoly Snigirev
European Synchrotron Radiation Facility, Grenoble, France

ABSTRACT

Synchrotron Radiation Workshop (SRW) - a physical optics computer code optimized for the simulation of emission and propagation of coherent and partially-coherent synchrotron radiation is presented. The code consists of two parts, which can be used independently. One part is dedicated to the computation of electric field, intensity, spectral-angular characteristics of radiation emitted by relativistic electrons in undulators, wigglers, short magnets, etc. The other part of the code implements physical optics methods for wavefront propagation. The propagation in free space is made according to the Huygens-Fresnel principle, by means of a prime-factor 2D FFT. Normal-incident optical elements are described by a complex transmission function. Fast algorithm for the propagation of electro-magnetic field through simple waveguides is implemented. The propagation of partially-coherent radiation is done by summing up contributions to the final intensity from different sources (e.g. from distinct emitting electrons), taking into account the sources' properties and applying, when possible, the convolution theorem with respect to intensity. SRW code can be used for physical optics simulations, design and optimization of refractive and diffractive optical elements for various spectral ranges, from far infrared to hard X-rays.

Keywords: physical optics, synchrotron radiation, wavefront propagation

1. INTRODUCTION

An outstanding feature of Synchrotron Radiation (SR) emitted by relativistic charged particles in magnetic fields of synchrotrons and storage rings is a very broad spectrum of wavelengths extending from far infrared to hard X-rays. The third-generation synchrotron radiation sources provide high flux, very high brightness and high degree of coherence of the radiation. Due to these features, the SR is currently a proven tool for research in many areas of science, from physics and chemistry to biology and medicine.

The main purpose of the SRW software project described in this paper is to provide users with a collection of computational tools for various practical applications of synchrotron radiation. To be able to construct a high-quality SR beamline which delivers radiation from a storage ring to a sample, one needs to know the characteristics of the emitted SR, such as spectrum, flux per unit surface (intensity), brightness, etc. Besides, one should be able to trace how the radiation wavefront transforms at propagation through various optical components, and what are the final characteristics of the radiation “on the sample”. The SRW code combines these two parts, i.e. it enables:

- high-accuracy computation of the SR emitted by an electron beam in a magnetic field of arbitrary configuration and treated in the near-field observation region;
- CPU-efficient propagation of wavefronts through optical elements (lenses, focusing mirrors, apertures) and drift spaces.

These two subjects were addressed separately by different authors, at different levels of approximation. The near-field SR computation was discussed in [1,2]. The topics related to the SR wavefront propagation were treated in [3-10]. We note that, in contrast to geometrical optics tools, the SRW implements the wavefront propagation using the methods of physical optics. This allows interference and diffraction to be treated, and the experimental techniques based on these and other wave-optics phenomena [11-15] to be optimized.

The computation methods for the SR emission and propagation implemented in code are briefly described in the next section. Section 3 presents several examples of the computation results obtained with the code. Finally, the advantages and limitations of the methods used in the code are summarized in section 4.

2. COMPUTATION METHODS AND IMPLEMENTATION

2.1 Synchrotron radiation in the near-field region

To compute synchrotron radiation emitted by a relativistic electron and observed in the near-field region, an approach based on retarded potentials can be applied. Starting from Fourier transformations of the retarded scalar- and vector-potentials [16], one can easily obtain the expression for the frequency domain electric field (Gaussian System) [2]:

$$\vec{E} = iek \int_{-\infty}^{+\infty} [\vec{\beta} - \vec{n}\,[1 + i\,(kR)^{-1}]]\,R^{-1} \exp[ik(c\,\tau + R)]\,d\tau, \tag{1}$$

where k is wave number, $\vec{\beta} = \vec{\beta}(\tau)$ instant relative velocity of the electron, $\vec{n} = \vec{n}(\tau)$ unit vector directed from instant electron position to an observation point, $R = R(\tau)$ distance from instant electron position to the observation point, c speed of light, e charge of electron.

Eq. (1) allows the computation of spectral characteristics and intensity distributions of practically any type of spontaneous emission in synchrotrons (i.e., conventional bending magnet SR, undulator and wiggler radiation), taking into account near-field effects. Besides, the electric field obtained from Eq. (1) contains all the amplitude and phase dependencies which are necessary for simulation of further wavefront propagation through optical elements and drift spaces in the framework of physical optics. In most cases, the observation distances are much larger than the radiation wavelength ($kR >> 1$), and the longitudinal component of the electric field in Eq. (1) can be neglected, so that only transverse electric field component ($\vec{E}_{\perp}$) needs to be considered.

2.2 Propagation of the wavefront from one electron

The synchrotron radiation emitted by one electron is intrinsically transversely coherent. Therefore, assuming that angles are small and distances are considerably larger than wavelength, the electric field of diffracted synchrotron radiation $\vec{E}_{\perp 2}$ can be computed from the electric field $\vec{E}_{\perp 1}$ at an aperture causing the diffraction by the well-known Huygens-Fresnel principle [17] (this can be shown by applying the integral theorem of Helmholtz and Kirchhoff to the electric field of synchrotron radiation given by Eq. (1)):

$$\vec{E}_{\perp 2} = -ik(2\pi)^{-1} \iint_{\Sigma} \vec{E}_{\perp 1}\, S^{-1} \exp(ikS)\, d\Sigma, \tag{2}$$

where Σ is a surface within the diffracting aperture, S is a distance from a point on this surface to an observation point. If Σ is (a part of) a plane perpendicular to the optical axis, and the observation points belong to another plane which is also perpendicular to the optical axis, then the Eq. (2) is a convolution type integral that can be quickly computed by applying the convolution theorem and 2D Fast Fourier Transforms. This gives a CPU-efficient method of propagation of the SR wavefront through a drift space.

The propagation of the transverse electric field through a perfect thin lens is described by a multiplication of the field by a quadratic phase-shifting transmission function [18]. For more complicated optical components, one can apply physical considerations or analytical methods (for example, the stationary phase method) to derive a proper transformation of the electric field from a transverse plane before the optical component to a plane immediately after it.

2.3 Radiation from finite-emittance electron beam

In most cases encountered in third-generation synchrotron radiation sources, the emission from individual electrons is not correlated, and the radiation wavelengths of practical interest are much shorter than lengths of electron bunches. Under these conditions, in order to obtain intensity distribution of the SR from a whole finite-emittance electron beam, one needs to sum up intensities of radiation from the individual electrons. Generally, the single-electron intensity I_0 obtained from the electric field of Eqs. (1),(2), depends on coordinates of the observation point, and also transverse coordinates, angles and energy of the emitting electron $(x, y; x_0, y_0, x_0', y_0', \gamma_0)$. The final intensity distribution is therefore:

$$I(x,y) = \int I_0(x,y;\ x_0,y_0,x_0',y_0',\gamma_0)\, f(x_0,y_0,x_0',y_0',\gamma_0)\, dx_0 dy_0 dx_0' dy_0' d\gamma_0, \qquad (3)$$

where *f* is particle distribution in the electron beam phase space.

For different types of emission and different optical schemes, the single-electron intensity I_0 may not depend strongly on some of the phase-space variables. In some cases, Eq. (3) is actually a convolution-type relation with respect to the observation and phase-space coordinates. Practical calculations are dramatically simplified in such cases.

Eqs. (1)-(3) allow simulation of many effects related to partial transverse coherence of synchrotron radiation. An alternative method of treating the propagation of the partially-coherent SR is based on Wigner distributions [4].

2.4 Implementation

The emission part of the SRW computer code contains a number of different methods implementing Eqs. (1) and (3) for optimized computation of various types of SR, including undulator and wiggler radiation, radiation from central parts and edges of bending magnets, etc.. An efficient high-accuracy generic method for computation of the emission from arbitrary transversely uniform magnetic field is also implemented.

The part of the code dedicated to the wavefront propagation is based on a prime-factor 2D FFT. The code possesses an automatic driver, which tries to keep the optimal sampling rate of the electric field at propagation through many optical elements and drift spaces. The propagation part of the code can be used with no direct relation to synchrotron radiation.

The code is written in C++, compiled as a shared library and interfaced to the "Igor Pro" scientific viewing / graphing package. MS Windows and Mac OS versions of the SRW code are freely available from the Web [19].

3. EXAMPLES OF COMPUTATION

3.1 Bending magnet SR: focusing and phase corrections

Consider a case of bending magnet SR at the following emission and observation conditions: electron beam energy of 2.5 GeV, current 0.5 A, zero transverse emittance; constant field in bending magnet of 1.56 T; photon energy 40 eV, horizontal angular aperture 6 mr, vertical aperture 4 mr (which is comparable to the natural opening angle of the bending magnet SR at this photon energy). Computed intensity distributions and phase corrections characterizing difference of the SR wavefront from that of a point source, are shown in Fig. 1. The phase correction for the vertical component of the electric field differs from the correction for the horizontal component by a π- flip at zero vertical position. This is a consequence of anti-symmetry of the vertical electric field with respect to the plane of the electron beam orbit.

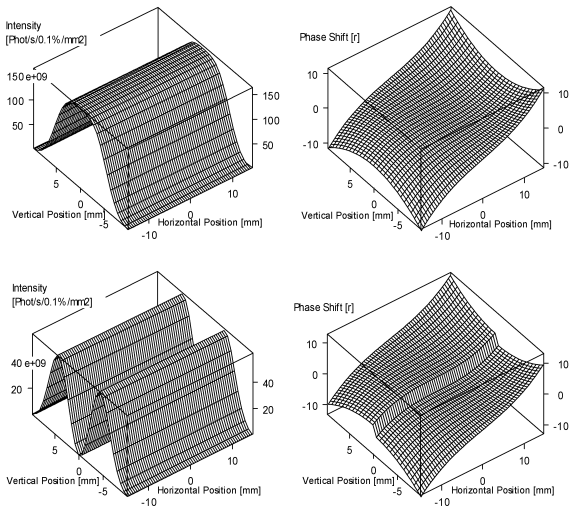

Figure 1. Left: intensity distributions of the bending magnet radiation in transverse plane at 5 m from the tangential “source point”. Right: phase corrections. Upper plots correspond to the horizontal, lower plots to the vertical polarization component of the bending magnet SR.

Consider now a 1:1 imaging scheme obtained by placing an ideal lens 5 m from the source. The computed intensity distributions in the image plane are presented in Fig. 2. Due to the phase differences of the bending magnet SR from that of a point source, there is an aberration in the focused spot, even though the focusing is performed by an ideal lens (left plots in Fig. 2). For a zero-emittance electron beam, this aberration appears when the horizontal aperture is comparable with the natural opening angle of the bending magnet SR, and it becomes larger as the horizontal aperture increases further. Due to the anti-symmetry of the vertical polarization component of the electric field, the corresponding intensity distribution appears split in the image plane (lower left plot).

Middle and right plots in Fig. 2 show the effect of the phase corrections. The phase corrections remove large secondary maximums of intensity distribution of the focused SR, reduce the spot size and increase the peak intensity values. The correction for the vertical electric field brings the main maximum of the intensity to the center of the focused spot (lower middle and right plots).

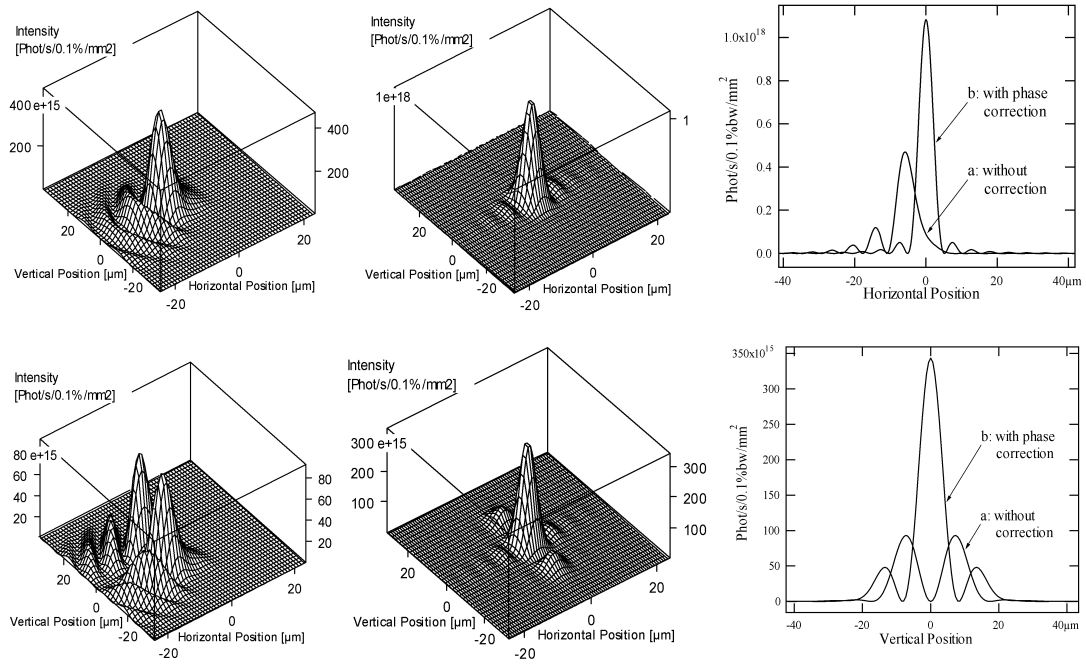

Figure 2. Intensity distributions of the focused bending magnet SR. Upper plots correspond to the horizontal, lower plots to vertical SR polarization component. Left: focusing by aberration-free "thin lens", without any phase correction. Middle: focusing with the phase correction applied at the longitudinal position of the lens (the correction is different for horizontal and vertical polarization components). Right: horizontal (for horizontal polarization component) and vertical (for vertical polarization component) cuts of intensity in the spot for the focusing without (a) and with (b) the phase correction.

3.2 Optimization of an infrared SR beamline

This example illustrates simulations of emission and propagation of infrared radiation in a realistic beamline in a high-energy storage ring. The beamline makes use of the radiation emitted at bending magnet edges (concentric ring pattern) and in the central part of a bending magnet. After passing through several limiting apertures located in the vacuum chamber of the storage ring, the wavefront is focused by a mirror in order to obtain the waist at the position of the CVD diamond window, which separates the initial high-vacuum part of the beamline. The wavefront is then collimated by another mirror, and propagates further though a drift space. Intensity distributions at 10 µm wavelength computed for different longitudinal positions along the beamline are shown in Fig. 3. The final intensity distribution contains both the intrinsic features of the edge radiation and the fringes resulting from diffraction in the beamline.

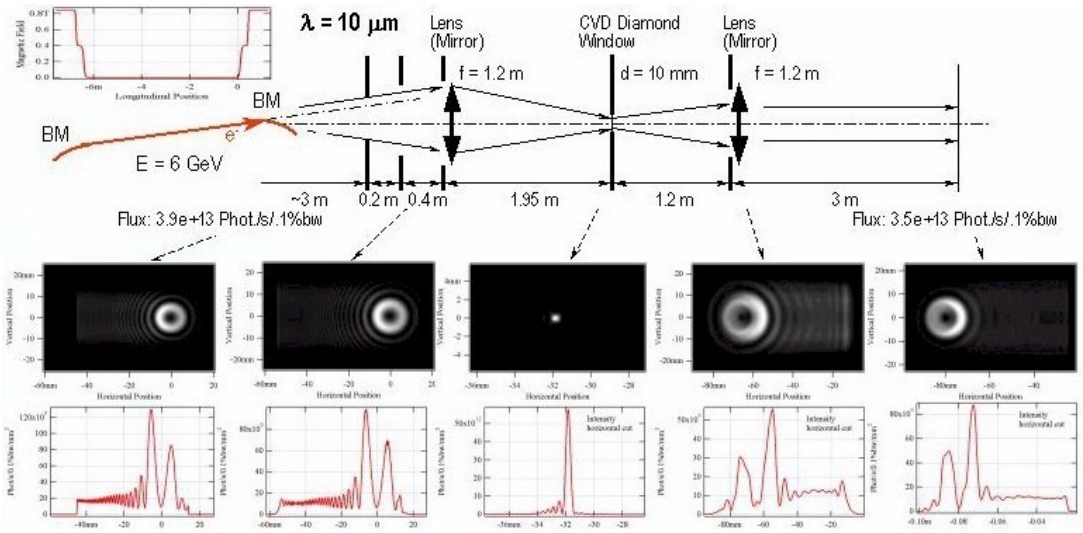

Figure 3. Simulation of emission and wavefront propagation of the infrared edge radiation (with the contribution of the SR from the central part of the bending magnet) for the conditions of the ESRF.

3.3 Simulation of X-ray focusing with compound refractive lenses

In this example, the X-ray focusing with Compound Refractive Lenses (CRL) [20] is simulated for two different cases of emission: the bending magnet SR (magnetic field of 0.85 T) at 8.9 keV photon energy, and the radiation from a planar undulator (38 periods of 42 mm) at 23 keV photon energy. The electron beam energy is 6 GeV in the two cases. The geometrical aperture of the CRL is 0.89 mm, the lens surface is a paraboloid of rotation, with minimal radius of 190 μm; the lens material is Al.

The computed single-electron intensity distributions in the plane before the lenses, immediately after the lenses, and in the image plane, are shown in Fig. 4. The computed FWHM sizes of the single-electron intensity distributions in the image plane are: 7.3 μm for 8.9 keV bending magnet SR, and 4.1 μm for 23 keV undulator radiation (lower right graph in Fig. 4). One can see from Fig. 4 that in the case of bending-magnet SR, the size of the focused spot is dominated by the apparent CRL aperture due to X-ray absorption in the lens material (attenuation length in Al is ~ 0.106 mm at 8.9 keV photon energy). For 23 keV UR, a contributing factor is also the size of the central cone of the undulator radiation, since the lens transmits this wavefront with only a small "shrinking" (attenuation length of Al is ~ 1.89 mm at 23 keV).

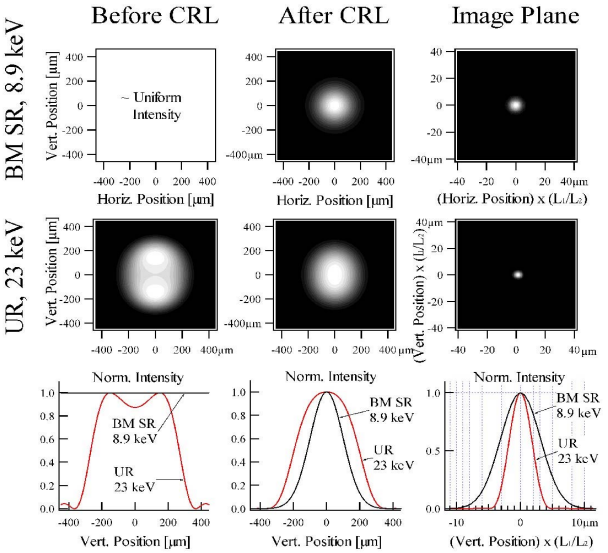

Figure 4. Computed intensity distributions of radiation emitted by one electron and focused by parabolic Al CRLs for two different cases of emission. Lower plots show the vertical cuts of the computed distributions, normalized by the maximum intensity. The horizontal and vertical positions in the image-plane plots (right) are scaled by the de-magnification factor, to show the distributions as for 1:1 imaging.

3.4 Interference and diffraction of partially-coherent X-rays

Two similar X-ray optical schemes are treated in this example: the classical scheme of Fresnel diffraction at a slit, and interference from a small boron fiber. In both cases, the radiation from a planar undulator (38 periods of 42 mm) at 11 keV photon energy is used. In the Fresnel diffraction scheme, a 100 µm x 100 µm rectangular slit is located at 37.6 m distance from the middle of the undulator, and the distance from the slit to detector is 5.5 m. In another scheme, a cylindrical boron fiber is placed at a distance of 40.6 m from the undulator, and the detector is located at a distance of 1.85 m after the fiber. The diameter of the fiber is 100 µm; the fiber possesses a tungsten core of ~15 µm in diameter.

The image plots of intensity distributions obtained in actual measurements in the two schemes are shown in Fig. 5. The vertical cuts of these intensity distributions are fitted by computation performed for these schemes according to Eqs. (1)-(3), with variable vertical size of the emitting electron beam. The fitting procedure allows actual vertical size of the electron beam to be determined [21].

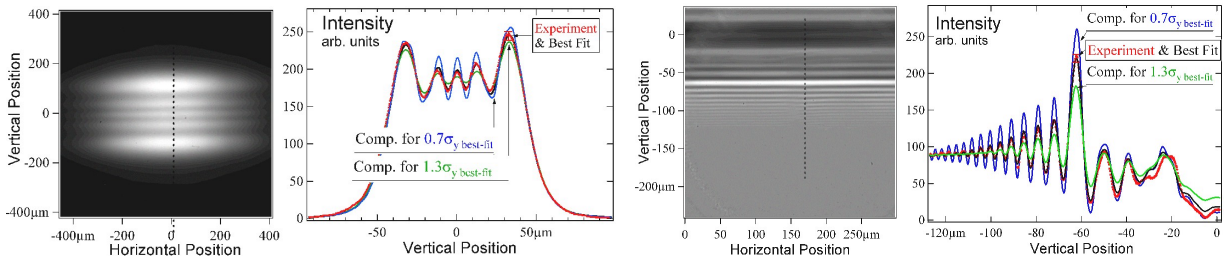

Figure 5. Measured intensity distributions and results of the fitting procedure for the Fresnel diffraction at a slit (left) and interference from a boron fiber (right).

4. ADVANTAGES AND LIMITATIONS

We emphasize the generality and high accuracy of the emission and wavefront propagation computation methods implemented in the SRW code. Magnetic fields of nearly arbitrary configurations are supported. The radiation can be computed at small distances from the emission region. The theoretical limits of the propagation are essentially those of the Fourier optics.

An advantage of the wavefront propagation method used in the code is speed. A featured wavefront can be propagated through several optical components and drift spaces within the time from seconds to minutes on up-to-date PC. This allows various optimizations of optical schemes.

When computing the SR propagation, one needs to sample the electric field of the wavefront over a sufficiently narrow grid in such a way that the phase shift between adjacent points is less than π. For short wavelengths and wide wavefronts this may require thousands of points in both the horizontal and vertical transverse directions, resulting in a very large consumption of memory. At this moment, this is the main limitation of the propagation method used in the SRW. Nevertheless, a number of practically important cases of wavefront propagation can be simulated for very short wavelengths, up to hard X-rays.

REFERENCES

1. R.P. Walker, “Near Field Effects in Off-axis Undulator Radiation”, *Nucl. Instr. and Meth.*, **A267**, p.537, 1988.
2. O.Chubar, “Precise computation of electron beam radiation in non-uniform magnetic fields as a tool for the beam diagnostics”, *Rev. Sci. Instrum.* **66**(2), p.1872, 1995.
3. A.Hofmann and F.Meot, “Optical resolution of beam cross-section measurements by means of synchrotron radiation”, *Nucl. Instrum. and Methods* **203**, p.483, 1982.
4. K.-J.Kim, “Brightness, coherence and propagation characteristics of synchrotron radiation”, *Nucl. Instrum. and Methods* **A246**, p.71, 1986.
5. A.Ogata, "On optical resolution of beam size measurements by means of synchrotron radiation", *Nucl. Instrum. and Methods* **A301**, p.596, 1991.

6. O.Chubar, “Resolution improvement in beam profile measurements with synchrotron light”, *Proc. of IEEE Particle Accelerator Conference PAC-93*, vol.**3**, p.2510, 1993.
7. N.V.Smolyakov, “Wave-optical properties of synchrotron radiation”, *Nucl. Instrum. and Methods* **A405**, p.235, 1998.
8. R.Bosch, “Focusing of infra-red edge and synchrotron radiation”, *Nucl. Instrum. and Methods* **A431**, p.320, 1999.
9. J.Bahrdt, “Wavefront propagation: design code for synchrotron radiation beamlines”, *Applied Optics* **36** (19), p.4367, 1997.
10. O.Chubar, P.Elleaume and A.Snigirev, “Phase analysis and focusing of synchrotron radiation”, *Nucl. Instrum. and Methods* **A435**, p.495, 1999.
11. A.Snigirev, I.Snigireva, V.Kohn, S.Kuznetsov and I.Schelokov, “On the possibilities of X-ray phase contrast micro-imaging by coherent high-energy synchrotron radiation”, *Rev. Sci. Instrum*. **66**(2), p.5486, 1995.
12. A.Snigirev, “Hard X-ray microscopy with coherent light: holography, phase contrast and interferometry”, *ICFA Workshop on 4th Generation Light Sources, Jan. 22-25 1996, ESRF, Grenoble*.
13. C.Raven, A.Snigirev, I.Snigireva, P.Spanne, A.Souvorov and V.Kohn, “Phase-contrast microtomography with coherent high-energy synchrotron X-rays”, *Appl. Phys. Lett.* **69**, p.1826, 1996.
14. P.Cloetens, R.Barret, J.Baruchel, J.P.Guigay and M.Schlenker, *J.Phys. D: Appl. Phys.* **29**, p.133, 1996.
15. T.E.Gureyev, C.Raven, A.Snigirev, I.Snigireva and S.W.Wilkins, *J.Phys. D: Appl. Phys.* **32**, p.563, 1999.
16. J.D.Jackson, *Classical Electrodynamics*, *2nd. ed., New York: Wiley*, 1975.
17. M.Born, E.Wolf, *Principles of Optics*, *4th ed., Pergamon Press*, 1970.
18. J.W.Goodman, *Introduction to Fourier Optics, 2nd ed., McGraw-Hill*, 1996.
19. http://www.esrf.fr/machine/groups/insertion_devices/Codes/software.html
20. A.Snigirev, V.Kohn, I.Snigireva, B.Lengeler, “A compound refractive lens for focusing high-energy X-rays”, *Nature*, **384**, p.49, 1996.
21. O.Chubar, A.Snigirev, S.Kuznetsov, T.Weitkamp, V.Kohn, “X-ray interference methods of electron beam diagnostics”, *Proc. of DIPAC-2001, May 13-15 2001, ESRF Grenoble*, p.88, 2001.